Chapter 3. The Wave Equation Approach to Multiples Modelling and Suppression

This chapter will be devoted to the implementation of the scalar wave equation as a descriptor of seismic wave fields. We will start by considering coordinate transformations that yield approximate equations for propagating up and downgoing waves in free space. Following this, we will couple up and downgoing waves to obtain equations valid for solving the forward or inverse problems. Finally, the theory will be illustrated with some synthetic examples.

The equations which we will deduce and solve in this chapter are

$$U'_{z't'} = -\frac{v}{2}\sec^3\theta U'_{x'x'} - c(x'z')D''_{t''}(x'-2\tan\theta\, z', z', t'-2\cos\theta\,\frac{z'}{v}) \quad (3\text{-}1a)$$

and

$$D''_{z''t''} = \frac{v}{2}\sec^3\theta\, D''_{x''x''} \quad (3\text{-}1b)$$

where $c(x',z')$ is the reflection coefficient, v the compressional velocity, θ the propagation angle and the subscripts denote partial derivatives. These equations represent the essence of the wave modelling and data processing schemes of this thesis and are thought to yield the most accurate deterministic multiple reflection suppression method of reflection seismic data processing. Nevertheless, it was still necessary to make many approximations. The derivation of (3-1a,b) will elucidate the accuracy of the approach. After completing it we will show how these equations are solved.

The inclusion of the wave equation in our scheme comes as a natural extension of our previous ray theory approximation. In effect, if we delete the term containing the second derivative in x, which is responsible for the diffraction of the acoustic energy, we are left within the framework of a ray approximation

$$U'_{z't'} = - c\, D''_{t'} \tag{3-2a}$$

$$D''_{z''t''} = 0 \tag{3-2b}$$

The first equation for U then can be integrated by t'. Representing the remaining derivative in z' through the difference $U_1 - U_2$ (omitting for simplicity the x', t' variables and assuming $Dz' = 1$), equation (3-2a) becomes $U_2 = U_1 + c_1 D_1$, which is equation (2-5a) of Chapter 2. On the other hand, equation (3-2b) implies D'' = constant, which corresponds to equation (2-5b). It is the possibility of including new properties such as diffractions and geometrical spreading which represents a major advantage over the simplified model of Chapter 2. However, important elements such as shear waves and absorption are still neglected.

We differentiate between two kinds of equations: the uncoupled and the coupled equations. The former refers to the equation that controls the propagation of each separate wave field (U or D) through a homogeneous region with no reflection or transmission effects. The latter describes the propagation through inhomogeneous media, where reflection coefficients couple up and downgoing waves.

Actually we have already obtained these two types of equations in Chapter 2, where (2-5b) was an uncoupled equation for D-waves and (2-5a) a coupled equation for U-waves. From their definition, as well as from the experience of Chapter 2, it follows that the structure of the coupled equations will be highly dependent on the model that we choose for the propagating medium.

3.1. Uncoupled Equations and Coordinate Transformations

There are two main objectives which we wish to accomplish through the coordinate transformation. First we want a transformation that yields separate equations for downgoing and upcoming waves. Second, we want a transformation which takes care of all spatial and temporal translations of the wave field, leaving the wave equation to do only diffraction.

It is not difficult to show that both objectives can be accomplished through the transformation

$$x' = x \pm z \tan\theta \tag{3-3a}$$

$$z' = z \tag{3-3b}$$

$$t' = \pm \frac{x \sin\theta}{v} \pm \frac{z \cos\theta}{v} + t \tag{3-3c}$$

where the sign "-" corresponds to downgoing waves, the "+" to upcoming waves and θ is the propagation angle (from the vertical) for a plane wave. If we refer only to downgoing waves and, as before, denote partial derivatives through subscripts so that

$$\frac{\partial^2}{\partial_x \partial_z} U = \partial_{xz} U = U_{xz} \tag{3-4}$$

then the Jacobian of this transformation can be written as

$$x'_{x,z,t} = 1, -\tan\theta, 0 \tag{3-5a}$$

$$z'_{x,z,t} = 0, 1, 0 \tag{3-5b}$$

$$t'_{x,z,t} = -\sin\theta/v, -\cos\theta/v, 1 \tag{3-5c}$$

By using (3-5), we can now transform the 2-D scalar wave equation

$$P_{xx} + P_{zz} - (1/v^2) P_{tt} = 0, \tag{3-6}$$

where P is the pressure, into the new coordinate system. Defining Q as the transformed wave field and noting that the wave field is invariant under coordinate transformations ($P(x,z,t) = Q(x',z',t')$), equation (3-6) becomes

$$v\sec^2\theta\, Q_{x'x'} + v\, Q_{z'z'} - 2v\tan\theta\, Q_{x'z'} - 2\cos\theta\, Q_{z't'} = 0 \tag{3-7}$$

The intermediate steps leading to (3-7) can be found in Appendix 1. In order to achieve the separation into U and D waves, we would like the obtained equation to be first order in z'. The standard procedure, known as paraxial or parabolic approximation, is to drop the $Q_{z'z'}$ term. The dispersion relationship of the remaining equation shows that its validity is then limited to an

aperture angle of approximately $\pm$ 15 degrees off the main direction of propagation θ . Besides, the same dispersion relation indicates that the term proportional to $Q_{x'z'}$ is only significant for angles of propagation larger than 40 degrees, which is, in any case, sort of an upper limit for the other more general approximations involved in the theory. Neglecting then both terms, equation (3-7) can be finally written as

$$Q_{z't'} = (v/2) \sec^3\theta \, Q_{x'x'} \tag{3-8a}$$

If we desire a better approximation to the wave equation than (3-8a), we could estimate $Q_{z'z'}$ from (3-8a) (after integrating by t' and differentiating by z') and substitute back into (3-7). However, to keep the discussion simple, we will leave equation (3-8a) as it is. It is interesting to notice that by choosing $z' = z \sec^3\theta$ we get:

$$Q_{z't'} = (v/2) \, Q_{x'x'} \tag{3-8b}$$

where the leading coefficient of $Q_{x'x'}$ is no longer angle dependent.

3.2. Coupled Equations

The equations that we obtained in 3.1 referred to waves propagating through a homogeneous region where up and downgoing waves are uncoupled. However, in order to solve the forward or inverse problem we have to consider the fact that the U and D wave fields will couple through the reflection coefficients of the medium.

For the case of stratified media, Claerbout [5] showed that the coupled equations for U and D waves can be written as

$$U_z = -(i\omega/v)\cos\phi\, U - (I_z / 2I)\,(U+D) \tag{3-9a}$$

$$D_z = (i\omega/v)\cos\phi\, D - (I_z / 2I)\,(U+D) \tag{3-9b}$$

In equations (3-9) U and D have been Fourier transformed in x and t, ϕ is interpreted as the deviation angle from the normal direction of propagation θ, and I is the impedance defined as

$$I = \rho\, v/\cos\phi \tag{3-10}$$

with ρ being the density. The use of equations (3-9) in our case is not totally justifiable since they are obtained by requiring that the medium characteristics be z-dependent only, whereas our theory allows for small lateral variations of the reflection coefficients. Nevertheless we will assume that they represent a reasonable approximation in the case of slowly varying media. This assumption will be reinforced at the end by the fact that, in the limiting case of a ray approximation, the coupled equations to be deduced from (3-9) give equations identical to those obtained in the previous chapter. The idea is then, to estimate ϕ as well as the Fourier transforms of U and D in relation to the frame of the waves of interest (U or D) . These estimations are substituted in (3-9) and the obtained equation is Fourier transformed back into the original frame. We will start by making the same assumptions of Chapter 2 in relation to the propagating medium, that is, we will ignore transmission losses (eliminates U from the second term in (3-9a)) and intrabed multiples (eliminates the second term completely in (3-9b)). Thus, as before, the only coupling that remains is in the upcoming wave equation

$$U_z = -(i\omega/v)\cos\phi\, U - (I_z / 2I)\, D \qquad (3\text{-}11)$$

We illustrate the above procedure with the transformation (3-5) for upcoming waves

$$x' = x + z \tan\theta \qquad (3\text{-}12a)$$

$$z' = z \qquad (3\text{-}12b)$$

$$t' = \frac{x \sin\theta}{v} + \frac{z \cos\theta}{v} + t \qquad (3\text{-}12c)$$

By requiring as before, that the wave fields be invariant ($P(x,z,t) = U'(x',z',t')$) and by using the Jacobian corresponding to (3-12), the first derivatives of U can be expressed in the new frame as

$$U_x = U'_{x'} - U'_{t'} (\sin\theta) / v \qquad (3\text{-}13a)$$

$$U_z = U'_{x'} \tan\theta + U'_{z'} + U'_{t'} (\cos\theta) / v \qquad (3\text{-}13b)$$

$$U_t = U'_{t'} \qquad (3\text{-}13c)$$

In order to estimate the Fourier transform of U_z and the wave-number-frequency relationships in both frames (observer and upcoming), we introduce in (3-13) a monochromatic solution of the type

$$\exp(ikx - i\omega t) \qquad (3\text{-}14)$$

We then obtain

$$ik\,U = (ik' + i\omega'(\sin\theta)/v)\,U' \tag{3-15a}$$

$$U_z = U'_{z'} + (ik'\tan\theta - i\omega'(\cos\theta)/v)\,U' \tag{3-15b}$$

$$-i\omega\,U = -i\omega'\,U' \tag{3-15c}$$

The cosine of ϕ in terms of the wavenumber k appears as:

$$\cos\phi = [1 - (\frac{kv}{\omega})^2]^{1/2} = [1 - (\frac{k'v+\omega'\sin\theta}{\omega'})^2]^{1/2} \tag{3-16}$$

Expanding (3-16) to the second order about $k'v/\omega'$, we obtain

$$\cos\phi \cong \cos\theta - \frac{k'v}{\omega'}\tan\theta - (\frac{k'v}{\omega'})^2 \frac{1}{2\cos^3\theta} \tag{3-17}$$

Its inverse to first order is

$$\cos^{-1}\phi \cong \cos^{-1}\theta\,[1 + \frac{k'v}{\omega'}\cdot\frac{\sin\theta}{\cos^2\theta}] \tag{3-18}$$

Inserting (3-13b) and (3-17) into (3-11) we obtain:

$$U'_{z'} = -\frac{v}{2}\sec^3\theta\,\frac{k'^2}{i\omega}\,U' - \frac{1}{2}\frac{I_z}{I}\,D \tag{3-19}$$

If now we differentiate (3-10) and substitute (3-18) into the expression for I and I_z, we get:

$$\frac{I_z}{I} = \frac{(\rho v)_z}{(\rho v)} + \frac{k'}{\omega'}\sec\theta\tan\theta\,v_z \tag{3-20}$$

The first term of this relation is associated with the reflection coefficient for vertical propagation, while the second term accounts for its angular dependence. Finally, to obtain the upcoming wave equation in time domain, we insert (3-20) into (3-19) and inverse Fourier transform

$$U'_{z',t'} = -\frac{v}{2}\sec^3\theta U'_{x',x'} - \frac{1}{2}\frac{(\rho v)_{z'}}{(\rho v)} D''_{t''} - \frac{1}{2} v_{z'}\sec\theta \tan\theta D''_{x''} \quad (3\text{-}21)$$

This equation is the coupled version of (3-8). The absence of the $U_{x',z'}$ term indicates that the approximations that were made when computing $\cos\phi$ and its inverse, left us within the scope of the approximation discussed in section 3.1. For practical purposes we would like equation (3-21) to be expressed in a single coordinate frame. That implies expressing D'' in terms of the upcoming coordinates x', z', t' . In order to do that we need the transformation between up and downgoing waves, which is:

$$x'' = x' - 2\, z' \tan\theta \quad (3\text{-}22a)$$

$$z'' = z' \quad (3\text{-}22b)$$

$$t'' = t' - 2\, z'(\cos\theta)\,/\,v \quad (3\text{-}22c)$$

Then equation (3-21) can be finally written as:

$$U'_{z',t'} = -\frac{v}{2}\sec^3\theta\, U'_{x',x'} - \frac{1}{2}\frac{(\rho v)_{z'}}{(\rho v)} D''_{t'}(x'-2z'\tan\theta, z', t'-2z'\cos\theta/v) -$$

$$- \frac{1}{2} v_{z'}\sec\theta\tan\theta\, D''_{x'}(x'-2z'\tan\theta,\ z',\ t'-2z'\cos\theta/v)\,. \quad (3\text{-}23)$$

To solve the forward or inverse problem we can complement the transformation (3-12) and the coupled equation (3-23) with the corresponding uncoupled equation for downgoing waves:

$$D''_{z''t''} = (v/2)\ \sec^3\theta\ D''_{x''x''} \quad . \tag{3-24}$$

Equations (3-23) and (3-24) are the equivalents of equations (2-7) in Chapter 2.

3.3. Computer Algorithms

The pair of equations (3-23) and (3-24) obtained in the last section suffice to solve the forward and inverse problem within the scope of the approximations involved. We will simplify the discussion further by assuming that the reflection coefficient is independent of angle. Neglecting then the last term in equation (3-23) and expressing the vertical reflection coefficient $(\rho v)_z/2(\rho v)$ as $c(x,z)$, equations (3-23) and (3-24) become

$$U'_{z't'} = -\frac{v}{2}\sec^3\theta\ U'_{x'x'} - c(x'z')D''_{t'}(x'-2\tan\theta\, z', z', t'-2\cos\theta z'/v) \tag{3-25}$$

and

$$D''_{z''t''} = \frac{v}{2}\sec^3\theta\ D''_{x''x''} \tag{3-26}$$

In order to use these equations as practical operators capable of extrapolating wave fields, either we have to find integral solutions for U and D or we have to approximate them through finite elements or finite differences. We shall take the last alternative. The first step in this direction is to discretize the coordinates and wave variables as we did in Chapter 2

$$x = j\,Dx \;;\quad z = k\,Dz \;;\quad t = n\,Dt \tag{3-27}$$

and

$$U(x,z,t) = U(j\,Dt,\ k\,Dz,\ n\,Dt) \;\text{---}>\; U^{n}_{k,j} \tag{3-28}$$

Since in equation (3-25) we have to express the downgoing wave in terms of upcoming coordinates we will need, in addition, the discrete version of the transformation (3-22) between U and D waves

$$j'' = j' - 2(Dz/Dx)\tan\theta\ k' \tag{3-29a}$$

$$k'' = k' \tag{3-29b}$$

$$n'' = n' - 2\,\frac{Dz}{v\,Dt}\cos\theta\,k' \tag{3-29c}$$

If we now define the sampling intervals Dx , Dz and Dt such that

$$2\tan\theta\ (Dz/Dx) = f \tag{3-30a}$$

and

$$2\cos\theta\,\frac{Dz}{v\,Dt} = e \tag{3-30b}$$

where f and e are integers, the transformation (3-29) reduces to

$$j'' = j' - f\,k' \tag{3-31a}$$

$$k'' = k' \tag{3-31b}$$

$$n'' = n' - e\,k' \tag{3-31c}$$

The next step is to introduce the unit delay operator $Z = \exp(-i\omega Dt)$ and the unit shift operator in the z direction $W = \exp(-ik_z Dz)$, such that

$$Z\, D^n_{k,j} = D^{n-1}_{k,j} \quad \text{and} \quad W\, D^n_{k,j} = D^n_{k-1,j} \tag{3-32}$$

With these definitions we can obtain by following the Crank-Nicholson scheme discrete centered approximations of the derivatives in z and t

$$D_z = \frac{\delta_z}{Dz} D = \frac{2}{Dz} \frac{1-W}{1+W} D^n_{k,j} \tag{3-33a}$$

$$D_t = \frac{\delta_t}{Dt} D = \frac{2}{Dt} \frac{1-Z}{1+Z} D^n_{k,j} \tag{3-33b}$$

For the second derivative in x we can use

$$D_{xx} = \frac{\delta_{xx}}{(Dx)^2} D = \frac{D^n_{k,j-1} - 2D^n_{k,j} + D^n_{k,j+1}}{(Dx)^2} \tag{3-34}$$

A better approximation results if, instead, we discretize the second derivative as

$$D_{xx} = \frac{1}{(Dx)^2} \frac{\delta_{xx}}{1 - b\,\delta_{xx}} D \tag{3-35}$$

where b is a constant which when made equal to $1/12$ gives fourth order accuracy in x. This may be important when working with real seismograms, where the data tends to be undersampled in x. Otherwise, b can be used to simplify the difference equations.

Substituting these difference approximations into equations (3-25) we will have

$$\frac{(1-Z)(1-W)}{(1+Z)(1+W)}\, U^{n'}_{k',j'} = -a\,\frac{\delta_{xx}}{1-b\,\delta_{xx}}\, U^{n'}_{k',j'} - \frac{1}{2}\, c_{k'j'}\, \frac{1-Z}{1+Z}\, D^{n''}_{k'',j''} \qquad (3\text{-}36)$$

where

$$a = \frac{v\ Dz\ Dt}{8(Dx)^2}\sec^3\theta \qquad (3\text{-}37)$$

With the help of (3-31) we can express D in the upcoming coordinates. If in addition we define a source term according to

$$S^{n'}_{k',j'} = (1/2)\, c_{k',j'}\, D^{n''}_{k'',j''} = (1/2)\, c_{k',j'}\, D^{n'-ek'}_{k',j'-fk'} \qquad (3\text{-}38)$$

and drop the primes, equation (3-36) becomes

$$(1-Z)(1-W)(1-b\delta_{xx})U^{n}_{k,j} = -a(1+Z)(1+W)U^{n}_{k,j} - (1-Z)(1+W)(1-b\delta_{xx})S^{n}_{k,j} \qquad (3\text{-}39)$$

Upon substituting (3-33), this equation can be rewritten as

$$[\,1+(a-b)\delta_{xx}\,]\,U^{n}_{k,j} = [\,1-(a+b)\delta_{xx}\,]\,(U^{n}_{k+1,j}+U^{n-1}_{k,j}) - [\,1+(a-b)\delta_{xx}\,]\,U^{n-1}_{k+1,j} -$$

$$-(1-b\delta_{xx})\,[\,S^{n}_{k+1,j} + S^{n}_{k,j} - S^{n-1}_{k+1,j} - S^{n-1}_{k,j}\,] \qquad (3\text{-}40)$$

Making $a = b$ (by properly choosing Dz or by dropping fourth order accuracy in x), equation (3-40) finally simplifies into an explicit equation

$$U^{n}_{k,j} = [\,1-2a\,\delta_{xx}\,]\,(U^{n}_{k+1,j}+U^{n-1}_{k,j}) - U^{n-1}_{k+1,j} - (1-a\,\delta_{xx})(S^{n}_{k+1,j} +$$

$$+ S^{n}_{k,j} - S^{n-1}_{k+1,j} - S^{n-1}_{k,j}\,) \qquad (3\text{-}41)$$

Another way to represent the delay operators in equation (3-36), is by rewriting it as follows

$$(1-W)(1-b\delta_{xx})U^n_{k,j} = -a\,\frac{(1+Z)(1+W)}{1-Z}\,\delta_{xx}U^n_{k,j} - (1+W)(1-b\delta_{xx})S^n_{k,j} \quad (3\text{-}42)$$

Now we can expand $(1-Z)^{-1}$ in a power series

$$(1-Z)^{-1} = 1 + Z + Z^2 + Z^3 + \cdots \quad (3\text{-}43)$$

Substituting back into (3-42) and letting as before $a = b$, we finish with an integrated form of equation (3-36)

$$U^n_{k,j} = (1-2a\delta_{xx})U^n_{k+1,j} - 2a\delta_{xx}\sum_{i=1}^{n}(U^{n-i}_{k,j} + U^{n-i}_{k+1,j}) -$$

$$- (1-a\,\delta_{xx})\,(S^n_{k,j} + S^n_{k+1,j}) \quad (3\text{-}44)$$

Similarly, the corresponding difference approximations for the uncoupled equation (3-26) are

$$D^n_{k,j} = (1 - 2a\,\delta_{xx})\,(D^{n-1}_{k,j} + D^n_{k-1,j}) - D^{n-1}_{k-1,j} \quad (3\text{-}45)$$

and

$$D^n_{k,j} = (1 - 2a\,\delta_{xx})\,D^n_{k-1,j} - 2a\,\delta_{xx}\sum_{i=1}^{n}(D^{n-i}_{k,j} + D^{n-i}_{k-1,j}) \quad (3\text{-}46)$$

A detailed discussion about the stability of these and other related equations can be found in [9]. I will just mention the two most

important constraints. First, the constant a has to be less or equal 4 ($a \leq 4$). Secondly, the only valid unknowns with time running forward are $U^{n+1}_{k,j}$ and $D^{n+1}_{k+1,j}$, while with time running backwards $-U^{n}_{k+1,j}$ and $D^{n}_{k,j}$. This last constraint is related to causality and has been discussed previously by Claerbout [5] and Riley [17].

Provided we guarantee stability, any of the equations presented here (3-41, 44, 45 and 46) can be used as a continuation equation to extrapolate up and downgoing waves from the surface back into the earth and vice-versa. I did not try to solve the inverse problem in the diffraction case, but the 2-D forward and 1-D inverse cases, indicate that the technique is closely related to that of Chapter 2. To implement the computer algorithm we have to supplement these equations with the corresponding initial and boundary conditions which, in principle, are identical to those of Chapter 2

$$U^{n}_{0,j} = R^{n}_{j} \tag{3-47a}$$

$$D^{n}_{0,j} = B^{n}_{j} - R^{n}_{j} \tag{3-47b}$$

$$U^{n}_{k,j} = 0 \quad \text{for} \quad n \leq k \tag{3-47c}$$

where, as before, R is the recorded surface seismogram and B is the source waveform. In addition, due to the presence of the diffraction term, we will need side boundary conditions. Here we have several choices: 1) we can assume that U and D vanish at the side boundaries, 2) we can assume a zero slope of the wave fields or, 3) if we want to avoid reflections off the sides, we can try the more sophisticated

absorbing boundary conditions discussed in [7]. For the computation of the synthetic examples shown in the next section, a zero slope condition was used. The remaining algorithm was close to that discussed by Riley with the exception that in the slanted case we have to consider an extra shift in x when comparing the U and D grids during the computation. Higher order algorithms are discussed in [10].

3.4. Synthetic Examples

Figure 3.1a shows the same model used in Chapter 2, that is, a dipping, undulating sea bottom, overlying a faulted reflector. The sequence illustrates only the forward problem. The vertical as well as the slanted seismograms are included. Although the computer algorithm used in this case was different from that of Chapter 2, the 1-D vertical and slanted seismograms (Figures 3.1b and 3.1c) are replicas of those obtained with the Noah algorithm. The only difference is in relation to the angle of propagation, which in this case allows for a better splitting of the peg-legs (PL_{11} through PL_{23}). The peg-legs at the right appear to separate due to lateral variations of the sea floor, while the peg-legs on the left clearly show distinct arrival times. The multiple reflections also show differences in arrival times when the vertical and the slant seismograms are compared. This is especially noticeable in the region where the second order multiple (M_2) intersects the faulted reflector (P_2) . The oscillations of the multiples in the slant case are smaller in amplitude compared to those of the vertical seismogram.

In the 2-D vertical seismogram (Figure 3.1d) we can observe the diffraction hyperbolas, which are usually symmetrical, in the regions where the acoustic energy focuses. Reflections are present as well, at the side boundaries due to the zero slope boundary condition that was used. Also a relatively large amount of numerical dispersion can be noted, indicating the need for better difference approximations. Comparison with the 2-D slant seismogram shows the loss of symmetry in the diffraction hyperbolas, which tend to be skewed and higher in amplitude toward the side from which they are being illuminated. The separation of the peg-legs is not as clear as in the 1-D case due to the masking by the diffractions.

Figure 3.2 is a repeat of the previous sequence but for a model that mimics a bright spot. Again, the complex separation of the peg-legs in the slanted case is clearly observed. The intersection of the second order multiple (M_2) with the top of the spot, also indicates differences in arrival times in both cases (vertical and slanted). In the 2-D seismograms (3.2d and 3.2e), the diffractions have the same asymmetrical pattern of the previous example.

Part II

THE PRACTICAL PROBLEM

Chapter 4. Wave Stacks

In the last two chapters we presented the basic theory for the modelling and suppression of multiples, and in the next two chapters we consider some aspects of the practical implementation of this theory. We will limit the discussion to the most fundamental points, which in our case are the source waveform estimation and the definition of valid input data. The former will be discussed in Chapter 5 while the latter is the subject of the present one.

In this chapter we will review Schultz's concept of wave stacks [21] as a means of defining data that is compatible with our assumptions and approximations. Following this, we will introduce the concept of optimum stacking intervals, which are the time windows over which the slant stack produces its most reliable results. This concept will help us to determine the values of the ray parameter p to choose in order to enhance a given sector of interest in the final stacked section. The chapter ends with a field data example.

Of the two problems considered by us, the forward and the inverse, it is the inverse problem that represents the practical interest. In effect, standard seismic exploration already furnishes us with the result of a real forward problem: the recorded seismograms. However, we must question whether these reflection seismograms can be considered as input data which are consistent with the assumptions of our theory.

The present theory in its two versions, 1-D and 2-D, was developed for plane waves propagating down or up from the earth. The data as recorded in the field in the form of a common shot point (CSP) gather do not fit this assumption, since they correspond to a propagating spherical wave. On the other hand, due to the improved quality and reduced amount of information, it would be desirable

to work directly with stacked sections as input data. In this sense we would like to think of the stacked section as an observed wave field, which is the product of a real physical experiment and thus, subject to physical equations such as the ones discussed in earlier chapters. Unfortunately, it is not difficult to realize that the standard stacked section -- the common midpoint (CMP) (also called common depth point (CDP)) section -- does not correspond to any physically realizable experiment and, therefore, cannot be used as input data in a deterministic procedure such as the one we are proposing. A new approach to this problem is described in the next paragraph.

4.1. Wave Stacks

Based on the superposition and reciprocity principles Claerbout [4] and Schultz [21] introduced the concept of Wave Stacks as a means to define data valid for wave equation processing. The idea behind this concept is that by stacking all the traces in a CSP gather we will be simulating the experiment of a geophone placed at the source location and shots placed at every geophone location which are fired in a pattern (time delays) defined by the stacking trajectories (Figure 4.1). If we just sum the traces without delays it would be equivalent to stacking along horizontal lines in the x,t plane (Figure 4.1a), and we will be simulating a horizontal plane wave propagating vertically along the z axis. If instead, we add along slanted lines (Figure 4.1b), we will be reproducing the result of a slanted wavefront. We could also think of adding along other lines in order to simulate more complex wavefronts. The same Reciprocity Principle allows for reversing the direction of propagation of the plane wave if we start from a common geophone gather instead of a CSP gather.

The important fact is that all these stacks can be interpreted as the result of a real experiment and therefore used as input data (more precisely, as boundary conditions) for a wave equation type of processing. Schultz [21] gives an extensive description of the details of these stacks and their practical implementation. I will just mention three points that are important for their actual computation.

1) In order to avoid aliasing due to the finite length of the Fresnel Zone (the region of coherent summation) along the stacking direction, an anti-aliasing window has to be introduced as shown in Figure 4.2.

2) It is necessary as well, to taper the data at both ends of the summation path to minimize end effects.

3) It is more advantageous to describe the wave stacks in terms of the ray parameter p ($p = \sin\theta/v$) than in terms of the propagation angle θ . The reason is that in the case of variable velocities, p remains constant while θ varies along the ray path.

The next section deals with the question of selecting the optimum parameters to produce a slant stack, corresponding to a slanted plane wave that leaves the surface at an angle θ .

4.2. Slant Stacks and Intervals of Optimum Stacking

The choice of different values of p will enhance different time intervals of a slant stacked section. This is because we are limited by several factors among which are: 1) the finite character of the data, especially along the x axis; 2) aliasing problems because of carrying the sum too far out off the Fresnel zone at some points; 3) the presence of the anti-aliasing window which, especially at early times, tends to restrict the sum to a region inside the Fresnel zone. Intuitively we

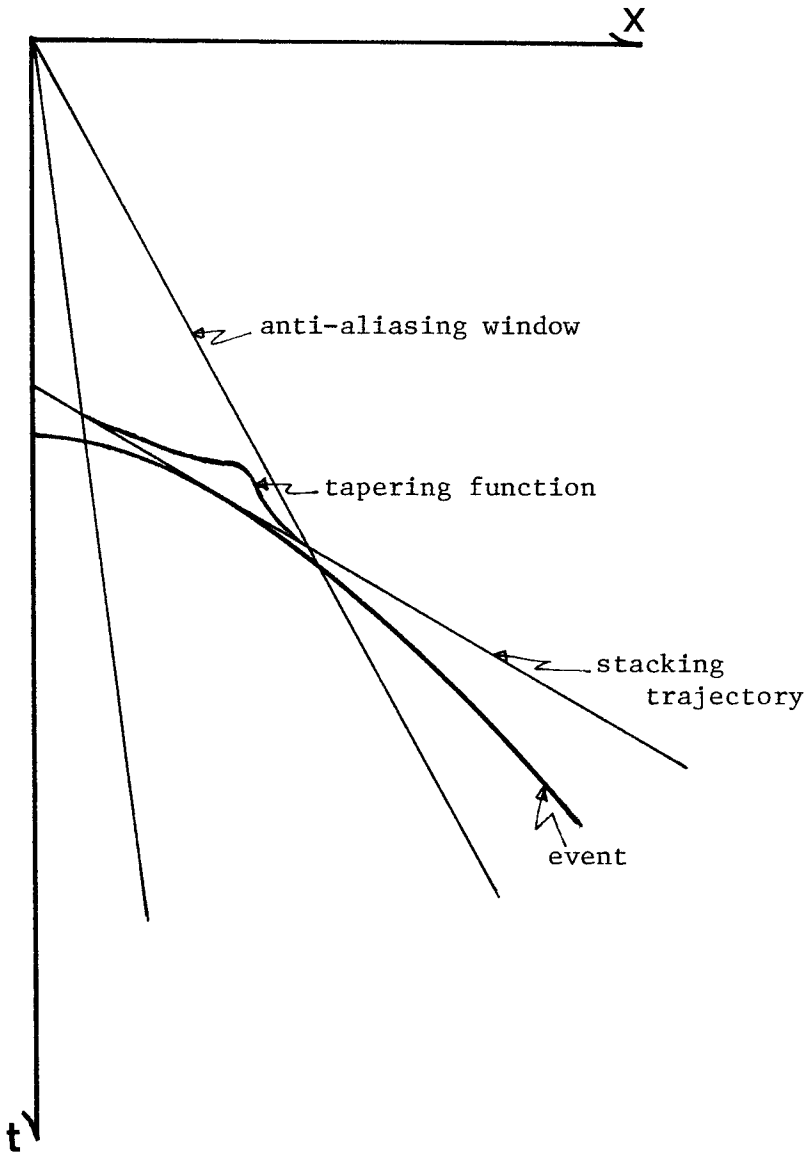

Figure 4.2. Anti-aliasing windows and tapering functions. Due to the finite extension of the Fresnel zone along the stacking path, an anti-aliasing window has to be introduced in order to avoid aliasing. Moreover, it is convenient to taper the sum at the extremes of the stacking line in order to minimize end effects.

may guess that larger values of p will yield better results at earlier times and vice versa. The idea then is to produce several p-stacks whose intervals of optimum stacking overlap and, on the whole, cover the full time axis. Afterwards, all these stacks could be combined linearly, applying weighting functions to each one, with maximum values along these intervals.

We will discuss the case of a constant-velocity, flat layered medium. For the simplicity of the mathematical equations, we will refer to the angle of propagation θ instead of the ray parameter p. Let us start by reviewing the equations used in the stacking process Figure 4.3):

$$t_p = f/pv^2 = (f/v)\sin\theta\,, \tag{4-1}$$

defines the direction of propagation;

$$t_s = t' + p\,f = t' + f\,\sin\theta/v\,, \tag{4-2}$$

defines the direction of stacking; and

$$t_e^2 = t_0^2 + f^2/v^2\,, \tag{4-3}$$

defines a given event (flat reflector). Additionally we have

$$t' = t_0\cos\theta\,. \tag{4-4}$$

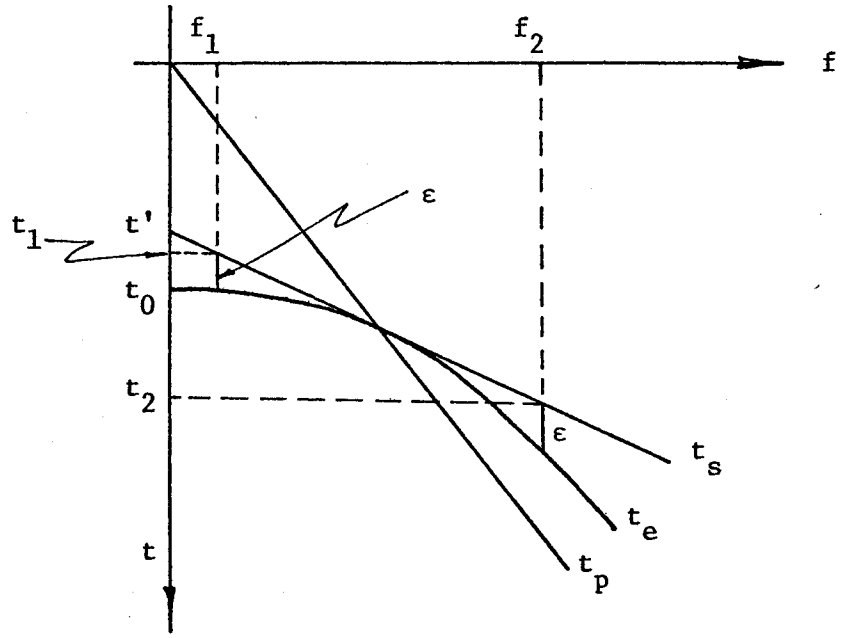

Figure 4.3. Slant stacks and Fresnel zones. The Fresnel zone is defined along the stacking line as a segment whose ends are half a period away (ε) from the reflection hyperbola (t_e). t_p is related to the ray parameter p and defines the point of tangency between the event arrivals (t_e) and the stacking path (t_s).

The Fresnel zone is then defined along the stacking path t_s as a region bounded by coordinates (f_1, t_1) and (f_2, t_2) such that the vertical distance ε (units of time) between t_s and t_e equals half the period of the source waveform. In order to define the boundaries of this zone, what we then need are equations for f_1 and f_2 (or t_1 and t_2) as functions of t' and ε. From Figure 4.1 and equations (4-2,3), after some algebra, we get

$$f_1(t') = (v/\cos^2\theta)\{\sin\theta(\varepsilon+t') - [\varepsilon(\varepsilon+2t')]^{1/2}\} , \qquad (4\text{-}5)$$

$$f_2(t') = (v/\cos^2\theta)\{\sin\theta(\varepsilon+t') + [\varepsilon(\varepsilon+2t')]^{1/2}\} , \qquad (4\text{-}6)$$

Further, we can make one of the two following assumptions:

1) We consider that, for a fixed f, ε increases linearly with time: $\varepsilon = \varepsilon_0 + bt'$ (ε_0, b-const.), so that the attenuation parameter $Q = \varepsilon/t' = \text{const.}$ (since $bt' >> \varepsilon_0$ most of the time), in which case (4-5,6) become

$$f_{1,2} = (v/\cos^2\theta)\{[1 + (1/Q)]\sin\theta \mp [1 + (2/Q)]^{1/2}\}\varepsilon . \qquad (4\text{-}7)$$

For larger t' these equations become straight lines and could define a natural anti-aliasing window.

2) We might also consider $\varepsilon = \text{const.}$ with time, in which case (4-5,6) become (assuming $\varepsilon >> t'$)

$$f_{1,2} \cong (\varepsilon v/\cos^2\theta)[t'\sin\theta \mp (2\varepsilon t')^{1/2}] . \qquad (4\text{-}8)$$

The shapes of these curves are illustrated in Figure 4.4. The first approach (Q = const.) will probably model better primary arrivals. For one of the waveform estimation techniques to be discussed in the next chapter, however, where only paths within the water layer are considered, we should take the second approach (ε = const.) .

Following these ideas, we will consider that portion of the stacking area that is inside the Fresnel zone and is bounded by the given data (the shaded area in Figure 4.4). This region defines an interval in time along the stacking axis $\Delta t' = t_2' - t_1'$ for which the summation will include only given data. If we want to compute this interval quantitatively, then we need inverse equations to (4-5,6) . That means t' as a function of f along the Fresnel curves

$$t_{1,2}' = (1/v)\tan^2\theta \{\varepsilon v + f \sin\theta \mp (\varepsilon v/\cos\theta)[1+(2 f \sin\theta/\varepsilon v)]^{1/2}\} \qquad (4\text{-}9)$$

For a given θ and a fixed offset, these solutions give two values of t along the stacking axis t' . Replacing f by F_1 , the initial offset of the gather, and by F_2 , the final (farthest) offset, in equation (4-9), we can then find the coordinates t_1' and t_2' which define the interval of optimum stacking in Figure 4.4.

As an example of practical interest, let us consider data for which F_1 = 200m, F_2 = 2550m (48 traces 50-m apart), and ε = 0.05 sec (for a 100-msec period waveform). The results for two different velocities v = 1500 m/sec and v = 2000 m/sec, are shown in Tables 4.1 and 4.2. Such tables eventually will allow us to choose the most

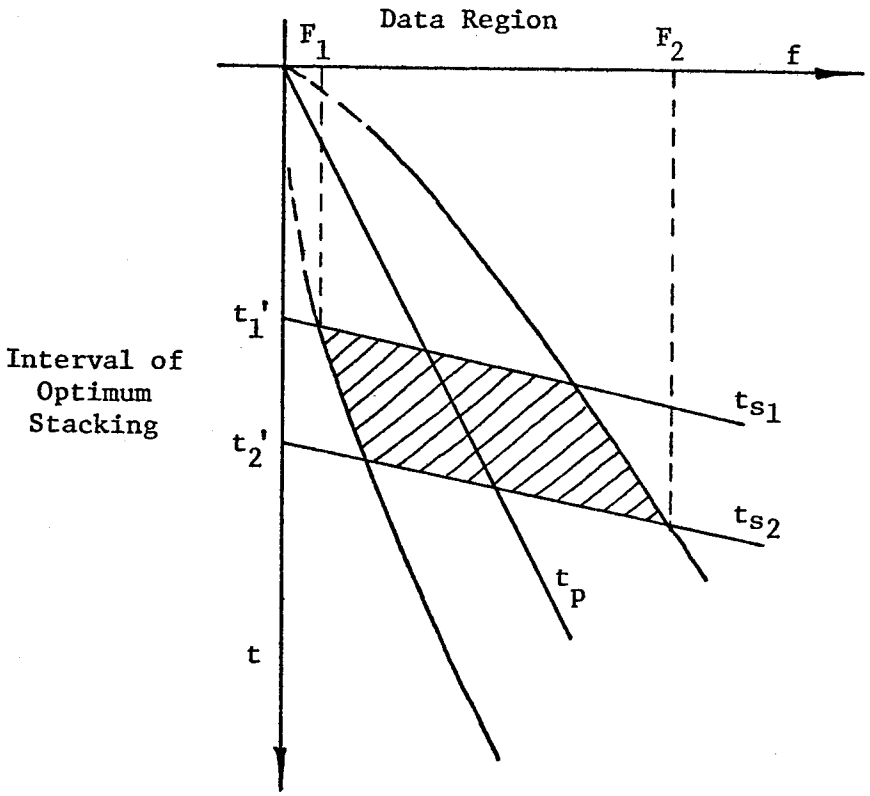

Figure 4.4. Intervals of optimum stacking. The slant stack will yield its best results in a time interval $t_1' - t_2'$ defined through the intersection of the Fresnel boundaries and the extreme offsets of the data (F_1 and F_2).

convenient propagation angle (p-value) for a given time interval of interest. We should mention here that these intervals could be increased by extrapolating traces at the left of F_1 and the right of F_2, but this would imply a good knowledge of velocity.

We could also define an interval of optimum stacking in relation to the anti-aliasing window, as that interval of the time axis within which our window includes the whole Fresnel zone but does not go too far off it (the shaded area in Figure 4.5). Without going through the algebra, we can find a relation that links t' and the distance δ between t_s and t_e at the boundaries of the stacking lines, given by the anti-aliasing window (Figure 4.6)

$$t'^{\pm} = (\cos\theta(1-\sin\theta \sin\theta^{\pm}) / \{[1+\sin\theta^{\pm}(\sin\theta^{\pm} - 2 \sin\theta)]^{1/2} - \cos\theta\}) \delta^{\pm} , \quad (4\text{-}10)$$

where $\theta^{+} = \theta + \Delta\theta$ and $\theta^{-} = \theta - \Delta\theta$.

When $\delta^{-} = \varepsilon$, the window will include the entire Fresnel zone. This condition defines our t'_1 in Figure 4.5. As the stack proceeds to later times, δ becomes larger than ε and aliasing will be introduced. We must then attempt to define a lower boundary t'_2 (Figure 4.5) by setting $\delta^{+} = r\,\varepsilon$ ($r > 1$) , such that within the interval from t'_1 up to t'_2 we have a tolerable amount of aliasing. As it turns out, $t'^{+} \simeq t'^{-}$ in relation (4-10), so by making $\delta^{+} = r\varepsilon$ we merely set $t'_2 = r\, t'_1$ (for a fixed θ and $\Delta\theta$). The choice of a particular value for r depends on how much aliasing we can tolerate. Table 4.3 contains the results for $r = 2$ (that means $\delta^{+} = 2\,\varepsilon$, the full waveform's period). This will set sort of a minimal interval of optimum stacking.

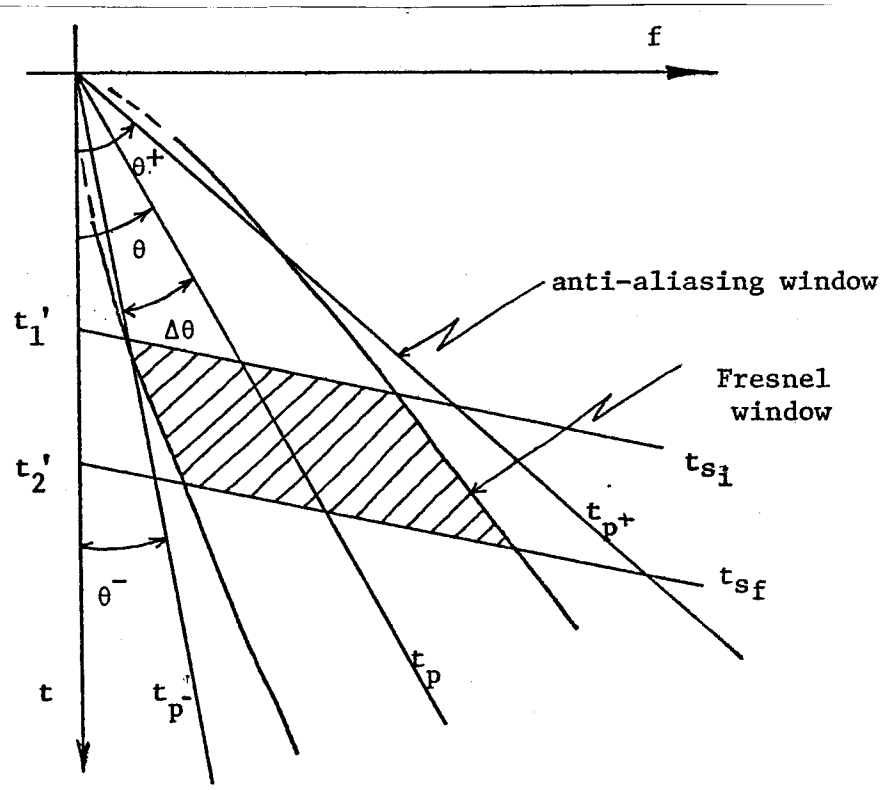

Figure 4.5. Anti-aliasing window and intervals of optimum stacking. Since the anti-aliasing and the Fresnel windows do not coincide, an interval of optimum stacking also can be defined in relation to the anti-aliasing window as the time interval for which both windows are close enough.

TABLE 4.1 (v = 1500 m/sec)

p (sec/m) $\times 10^{-4}$	θ (deg)	t_1' (sec)	t_2' (sec)	Dt' (sec)
0.58	5	15.99	8.63	0.00*
1.16	10	4.62	5.26	0.64
1.73	15	2.30	3.70	1.40
2.28	20	1.40	2.80	1.40
2.82	25	0.95	2.15	1.20
3.33	30	0.68	1.68	1.00
3.82	35	0.50	1.30	0.80
4.29	40	0.39	1.00	0.60

*No solution

Table 4.1. Intervals of optimum stacking for different p-values. t_1' and t_2' are the beginning and the end of the intervals respectively. Dt' is their extension. The values displayed correspond to data for which the nearest offset is 200m and the farthest 2550m (48 traces, 50m apart). ε is considered to be .005 sec (100 ms period waveform) and the velocity equal to 1500m/sec.

TABLE 4.2 (v = 2000 m/sec)

p (sec/m) $\times 10^{-4}$	θ (deg)	t_1' (sec)	t_2' (sec)	Dt' (sec)
0.44	5	15.30	5.75	0.00*
0.87	10	4.30	3.60	0.00*
1.29	15	2.09	2.57	0.48
1.71	20	1.25	1.94	0.69
2.11	25	0.84	1.50	0.66
2.50	30	0.60	1.17	0.57
2.87	35	0.44	0.91	0.45
3.21	40	0.34	0.70	0.36

*No solution

Table 4.2. Same as Table 4.1 but for a velocity of 2000 m/sec.

If tables like 4.1 and 4.2 allow us to choose the best value of θ (or p) for a given time interval, tables like 4.3 will allow us to choose the more convenient window. Finally, we may remark that the anti-aliasing window does not have to be symmetrical. In any case, relation (4-10) can easily be extended to incorporate such an eventuality.

Figure 4.7 includes three different stacks of real data. For the computation, I have assumed a velocity of 2000 m/sec, which is a lower bound of the actual velocities in the section. According to Table 4.2, for an angle of propagation of 20° (shallow depths), we shall expect an interval of optimum stacking that goes from 1.25 to 1.94 sec. As can be seen from Figure 4.7(c), this prediction correlates pretty well with the shown section. Figures 4.7 (a,b) correspond to angles of 10° and 15° . Here we are considering greater depths where the velocities are on the order of 4000-5000 m/sec; thus, Table 4.2 is no longer a good approximation, and we see that the intervals of optimum stacking are higher (in time) than the predicted values.

4.3. A Field Example

As a final illustration of slant stacks we present a more detailed analysis of the data introduced in Tables 3.1 and 3.2. The data set is a marine seismic reflection line, collected in the Gulf of Alaska. The data was originally furnished in the form of 48 trace CSP gathers with a geophone spacing of 50 m . In the next chapter we will be concentrating on a piece of this data where the first sea bottom reflection arrives around 1.2 sec and the corresponding multiple around 2.4 sec. Hence, we will slant stack the data in such a way that the interval of optimum stacking is tuned to the time interval containing the first

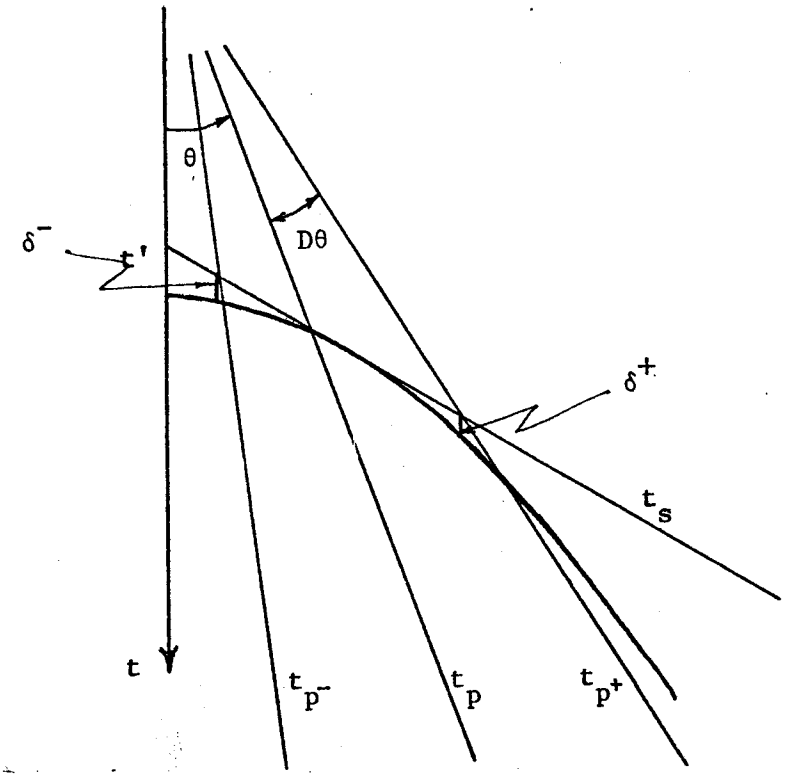

Figure 4.6. Anti-aliasing windows and reflection events. While the separation ε between the extremes of the Fresnel boundaries and the reflection hyperbolas is the same at both ends, the separation δ between the anti-aliasing window and the same events may not be equal at both ends.

TABLE 4.3

θ (deg)	$D\theta$ (deg)	t_1' (sec)	t_2' (sec)	Dt' (sec)
10	10	3.24	6.48	3.24
15	10	3.12	6.24	3.12
15	15	1.42	2.84	1.42
20	10	2.95	5.90	2.95
20	15	1.34	2.68	1.34
20	20	0.78	1.56	0.78
25	10	2.75	5.50	2.75
25	15	1.25	2.50	1.25
25	20	0.73	1.46	0.73
25	25	0.48	0.96	0.48
30	10	2.51	5.02	2.51
30	15	1.14	2.28	1.14
30	20	0.67	1.34	0.67
30	25	0.44	0.88	0.44
30	30	0.32	0.64	0.32
35	10	2.25	4.50	2.25
35	15	1.03	2.06	1.03
35	20	0.60	1.20	0.60
35	25	0.40	0.80	0.40
35	30	0.30	0.60	0.30

Table 4.3. Intervals of optimum stacking for different anti-aliasing windows. θ is the propagation angle, $D\theta$ is the width of a symmetrical window around θ. t_1', t_2' and Dt' have the same connotation as in Tables 4.1 and 4.2 .

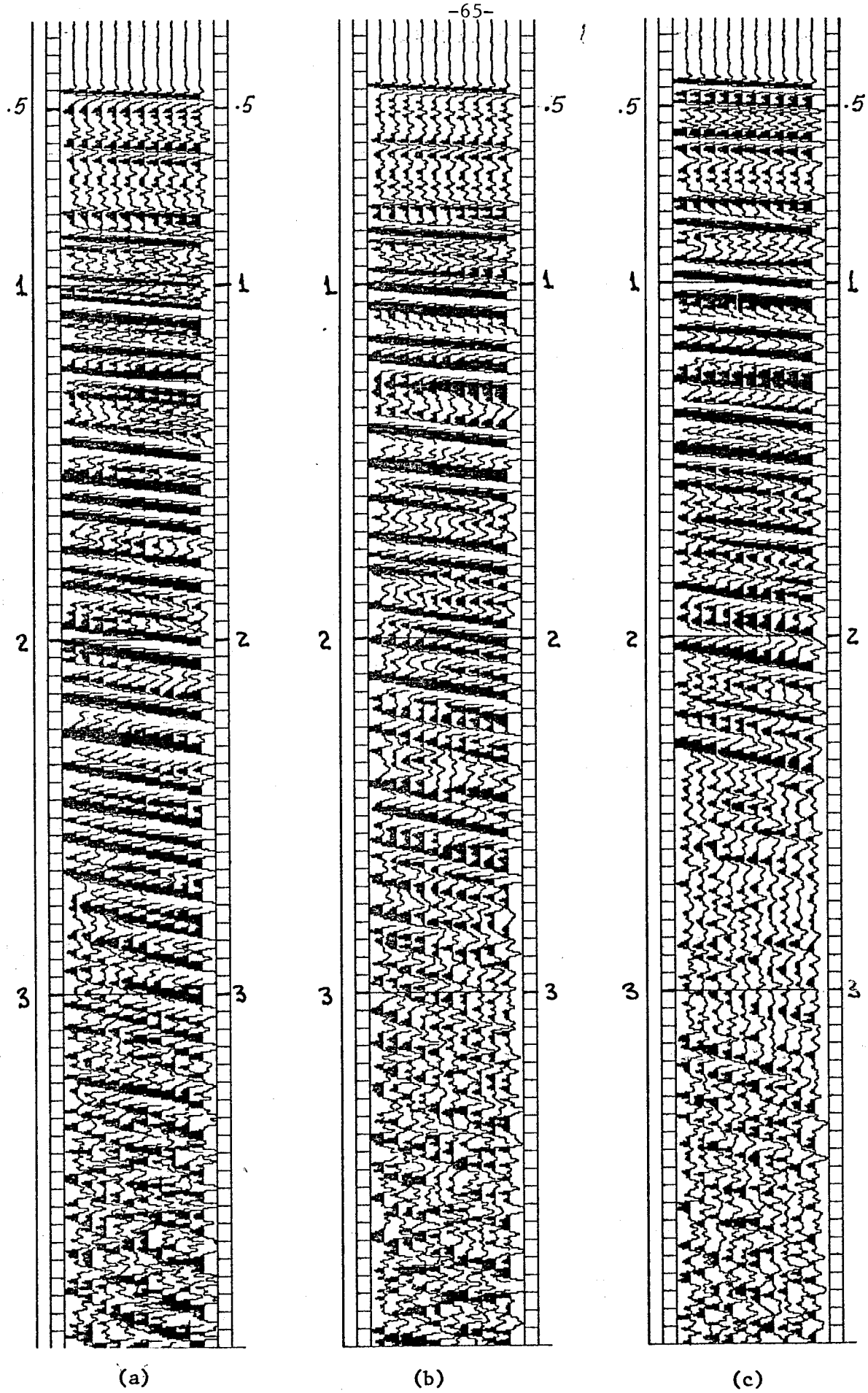

FIGURE 4.7—(a) Slant stack for v = 2000 m/s, θ = 10° (p = 0.87×10^{-4} s/m);
(b) Slant stack for v = 2000 m/s, θ = 15° (p = 1.29×10^{-4} s/m);
(c) Slant stack for v = 2000 m/s, θ = 20° (p = 1.71×10^{-4} s/m).

primary and its corresponding multiple. These two reflections involve only paths within the water layer, so the assumption of a constant velocity of about 1500 m/sec should be a good approximation. According to Table 4.1 the best p-value for this time interval is $p = 2.28 \times 10^{-4}$ sec/m which implies a departure angle of 20 degrees for the slanted wave. For this choice of p the interval of optimum stacking lies between 1.4 and 2.8 seconds. Table 4.3 indicates an anti-aliasing window aperture between 10° and 15° should be used.

The original data was slant stacked with the parameters outlined above and the result is shown in Figure 4.8. Besides the anti-aliasing window, a tapering function (a cosine bell) was applied along the stacking trajectory. The resulting section simulates the reflections from a slanted plane wave propagating from left to right at an angle of 20° as indicated in the upper left corner of this figure. The effects of the slanted propagation can be noticed in at least two instances. They are:

1) In region A, at the end of the slope (1.2 sec), the first multiple (A') is shifted almost 20 traces in the direction of propagation.

2) The diffraction hyperbolas (h) are clearly skewed and larger in amplitude toward the side of the source (left side). This is the same effect present in the 2-D synthetics of Figures 3.1 and 3.2.

Finer effects such as the multiples arriving at times that are not equal to twice the primary arrival times are discussed in the next chapter.

Figure 4.8. Slant stacked section for a plane wave propagating from right to left at an angle of 20° from the vertical. The values for p ($p = 2.28 * 10^{-4}$ sec/m) and the width of the anti-aliasing window ($\pm$ 15°) were chosen to enhance the time interval from 1.2 to 2.4 sec. Notice that the diffraction hyperbolas (h) are skewed and larger in amplitude toward the left as in the 2-D synthetics of Figure 3.1 and 3.2. The section is displayed in the slanted frame, so the end of the slope of the multiple (A') is shifted almost 20 traces to the right from the corresponding point on the primary (A).

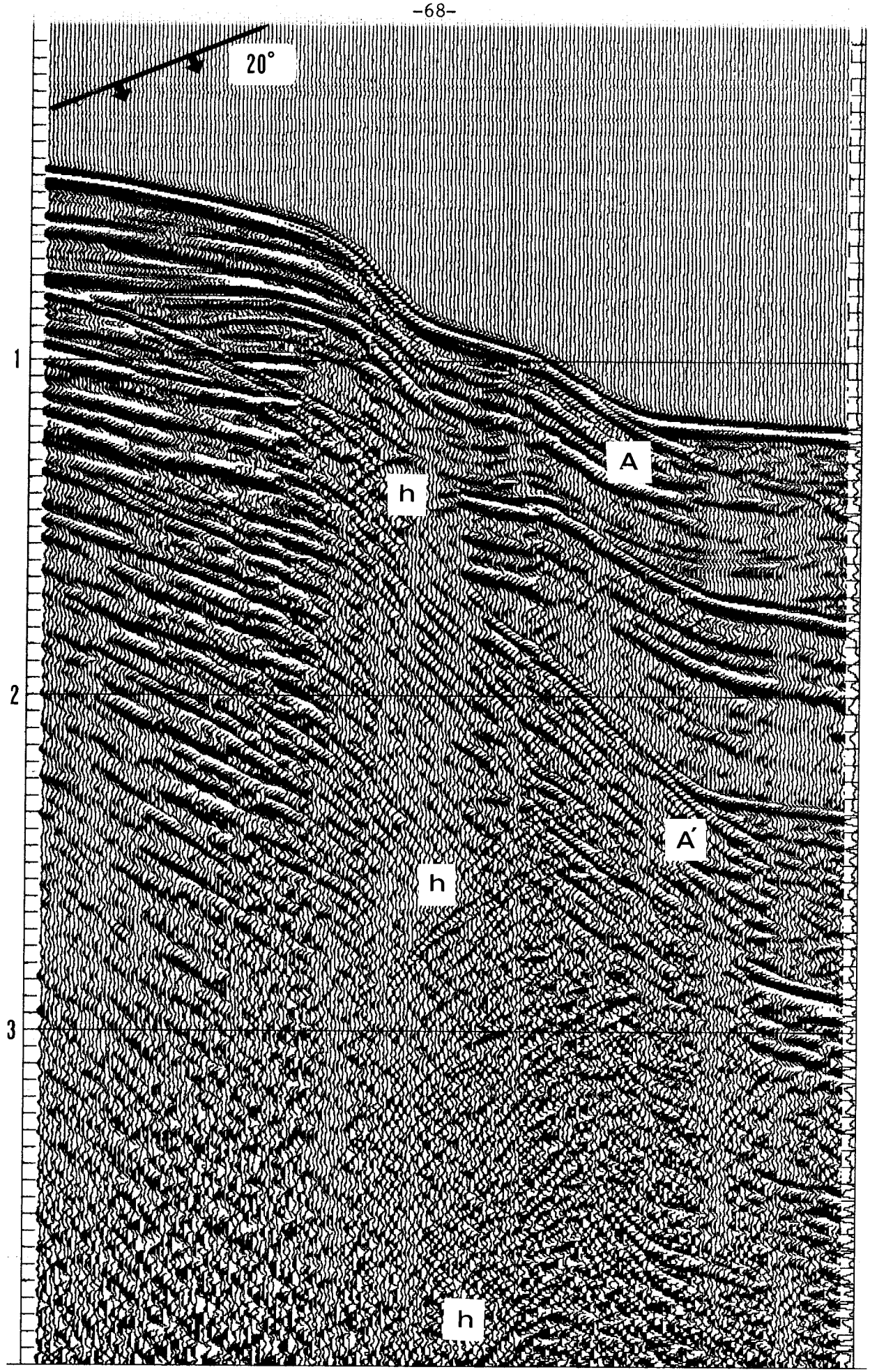

Figure 4.8

For comparison, Figure 4.9 displays a slant stacked section for $p = 1.16 \times 10^{-4}$ sec/m ($\theta = 10°$) and anti-aliasing window asymmetrically centered around θ (-10°, +15°) . The shift between A and A' for this case is of about 10 traces and the diffraction hyperbolas are almost symmetrical in relation to the t-axis .

Figure 4.9. Same as Figure 4.8 but for an angle of propagation of 10°. In this case the diffraction hyperbolas are almost symmetric and the shift between A and A' is about 10 traces.

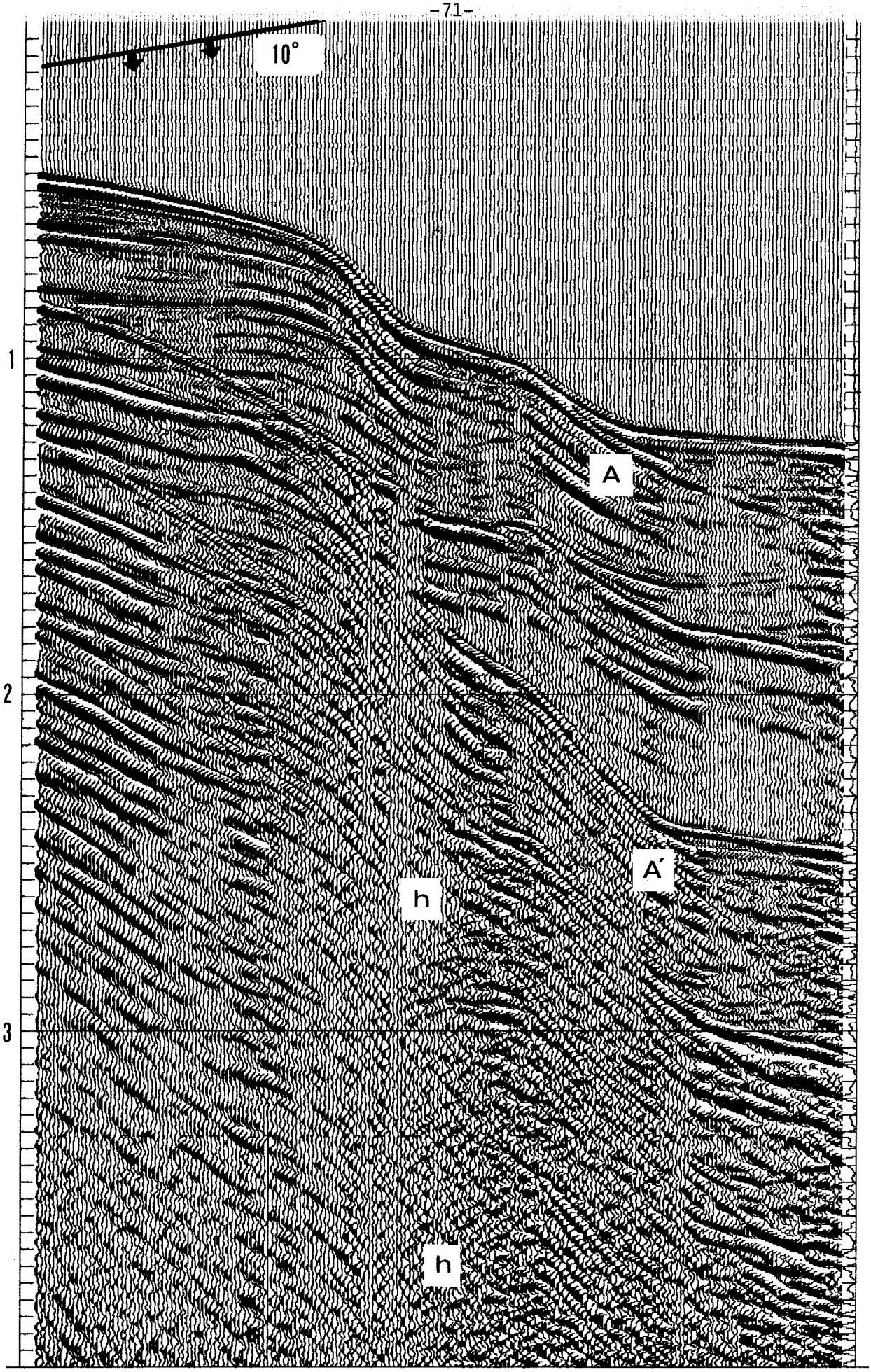

Figure 4.9